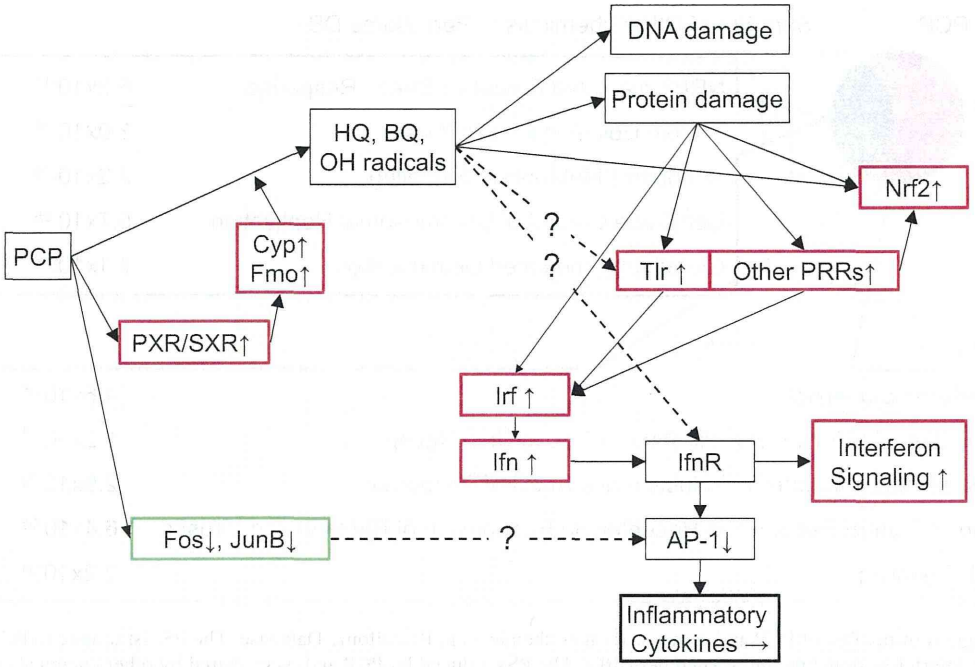

Fig. 8. Tentative summary scheme of the PCP induced networks in mouse liver. PCP or its metabolites may stimulate PXR/SXR or CAR, thereby inducing Cyp2, 4, 7, Fmo2, 5 within 8 hr to facilitate PCP metabolism, generating HQ (TCoHQ,TCpHQ), BQ (TCpBQ) and hydroxyl radical. The metabolites/radicals induce DNA damage and Protein damage. These reaction triggers Nrf2 networks and PRR system, initiating Irf mediated synthesis of Interferon alpha, which triggers the interferon signaling networks by autocrine or paracrine mechanisms. On the other hand, there remains a possibility that the metabolites may act as direct ligands to Tlr or IfnR and trigger downstream events as indicated in dotted lines with "?". Before activating interferon signaling networks, PCP suppressed Fos and JunB, which might have suppressed the inflammatory cytokine induction as shown in dotted line with "?".

accompanying distinct induction of Keap1, and other metabolic pathways (Figs. 5 and 6, Supplementary Table 1). Those networks were in the Common list mentioned above. Other networks were not effectively identified by the Ingenuity pathway analysis.

DISCUSSION

Among the chemicals tested in the Percellome project, PCP was slow to induce changes in gene expression; only around one hundred PSs were induced before 8 hr and 1,200 PSs at 24 hr. It would be plausible to hypothesize that PCP was metabolized during the first 8 hr and that the metabolite(s) then induced the 24 hr burst of ISGs and Nrf2-mediated genes. The time course of PCP action is in accord with the reported biological half-life of PCP; 6 to 27 hr in rodents (Larsen *et al.*, 1972; Braun *et al.*, 1977). A few metabolizing enzymes located downstream of PXR/SXR were induced during the first 8 hr (Fig. 3). The presence of DEHP in the top part of the common chemical list in Table 1 is also consistent with this hypothesis.

It would be of interest to ascertain whether PCP or its metabolite(s) could be PXR/SXR ligands. Metabolites known are tetrachloro-p(o)-hydroquinone (TCpHQ and TCoHQ) and tetrachloro-p-benzoquinone (chloranil, TCpBQ). Further, TCpHQ is reported to be metabolized, generating hydroxyl radicals with a help of H_2O_2 without Fenton reaction, to trichloro-hydroperoxyl-1,4-benzoquinone (TrCBQ-OOH) and trichloro-hydroxy-1,4-benzoquinone (TrCBQ-OH) (Zhu and Shan, 2009). We have no Percellome data of those metabolites and, to date, there are no reports on the interaction of PCP or its metabolites with the PXR/SXR. There are reports that PCP affects the function of estrogen receptor (Jung *et al.*, 2004) and thyroid hormone receptor (Kawaguchi *et al.*, 2008). Further study will be needed to identify the triggering event for the earliest responses to PCP.

Hepatocarcinogenic activity of PCP has been shown by rodent studies (NTP, 1999). The metabolites of PCP mentioned above were considered as the cause of oxidative stress or the hydroxyl radical insults against the liver (Zhu and Shan, 2009; Tasaki *et al.*, 2012).

It was reported that Tlr4-mediated, lipopolysaccharide-induced activation of the Ifn-β promoter was inhibited by PCP in a Myd88-independent way (Ohnishi *et al.*, 2008). On the other hand, PCP was considered to trigger Tlr4 via the induction of hydroxyl radicals (Lucas and Maes, 2013). In our experiment, PCP had significantly up-regulated Myd88, Irak1, Traf6, Tlr2, Tlr3, Tlr5, Tlr9 at 24 hr. Although the induction did not reach statistical significance, Tlr4 expression was also elevated. In addition, Irf 3, Irf7 and Irf9 were also induced. These findings might indicate that the TLR system was triggered by PCP itself, its metabolites or hydroxyl radicals via modifying the cytoplasmic proteins; abnormal proteins might be sensed by the TLRs or the pattern recognition receptors (PRR) system. Since Irf3, 7, 9 and Ifn-α1 expression are also increased, it could be possible that Irf mediated autocrine or paracrine of the Ifn-α is triggered, resulting in a burst of ISGs, as postulated by Sato *et al.* (Sato *et al.*, 2000).

Although Myd88 is mobilized, NF-κB, TNF, IL12 and CD40 were not induced, indicating that there may be a switch towards inflammatory cytokine production that was not directly induced by PCP. In relation to the switching mechanism, there is a report that isopropanol impaired AP-1 activation by removing Fos and JunB from the nuclear region of monocytes *in vitro* and suppressed Tlr4-mediated lipopolysaccharide stimulated Tnf-α production (Carignan *et al.*, 2011). In our data, Fos/JunB was down-regulated at earlier phase. As this change might correspond to AP-1 suppression (Gomard *et al.*, 2010), one possibility could be that PCP itself (as an alcohol/phenol) inhibited inflammatory cytokine production.

In contrast to the possible indirect mechanisms noted above, there are two examples that lead us to consider a possibility of direct activation of the ISGs. The first example is a low-molecular weight compound "imiquimod", a Tlr7 agonist, already on the market for treatment of skin viral infection (Hemmi *et al.*, 2002). Subcutaneous injection of imiquimod was reported to induce fever, sickness behavior and induction of ISG in rats (Damm *et al.*, 2012). The second example is a new polyfluoromethylated compound, 8-(1, 3,4-oxadiazol-2-yl)-2, 4-bis (trifluoromethyl) imidazo [1, 2-a] [1, 8] naphthyridine (RO4948191) which was reported to be an orally available low molecular weight interferon receptor agonist. RO4948191 was shown to induce a set of ISGs (Konishi *et al.*, 2012), such as Oasl, Adar, Bstl, Statl, Ifit3, Usp18, Isg15, Herc6 and Cxcl10. These two examples of direct ligands to TLR and IFNR lead us to hypothesize that PCP and/or its metabolites may be able to directly activate these receptor systems (Fig. 8). Further investigation will be needed to clarify the molecular mechanism(s) through which PCP administration triggers the ISGs. It is tempting to speculate that this classic toxin, PCP, could be used as a new lead for orally applicable interferon-manipulating and/or cytokine switching drugs.

Hyperthermia or hyperpyrexia, profuse sweating, uncoordinated movement, muscle twitching, and coma are reported in humans and experimental animals as acute symptoms of PCP poisoning. These functional symptoms were reported to be caused by the mitochondrial uncoupling effect of PCP. Ucp2 and Ucp3 and some mitochondrial genes are induced in this study (Supplementary Table 2, Supplementary Fig 1). These genes are supportive for uncoupling effect. However, many of the Krebs cycle enzymes were not induced and those that were induced showed very small increases compared to the induction of ISGs. Some peroxidases were also mildly induced, but catalase was not induced by PCP. In the Percellome database, chemicals reported as uncouplers are aspirin, ethanol, sodium arsenite, and 2,4-dinitrophenol. Under the current computational condition, none of them was picked up as a chemical sharing PS list with PCP.

Taken together, our data may be interpreted to indicate that the functional symptoms represented by hyperthermia can be induced by PCP mainly through the activation of ISGs. This interpretation is backed up by the literature on "endogenous pyrogens" (Dinarello, 1999) and on imiquimod (Damm *et al.*, 2012).

Finally, although not yet perfected, the performance of the RSort and PE programs were demonstrated to be sufficient to sort out biologically meaningful changes for the comprehensive characterization of PCP. Manual searches employing different criteria added about 100 mildly changing PSs (data not shown), but the conclusions of our study were not affected. Nevertheless, further refinement for the better coverage is underway.

In conclusion, the RSort program-based comprehensive cross-reference of the Percellome database revealed that PCP was the only chemical among 111 orally administered chemicals that significantly induced the ISGs in hepatocytes. *In situ* hybridization confirmed that the parenchymal hepatocytes are responding to PCP. Two possible mechanisms were discussed; indirect mechanism via the PRR system, and direct stimulation of the Tlr(s) or IfnR(s). Further study is needed to clarify the possible molecular mechanisms.

ACKNOWLEDGMENTS

The author thanks all the member of the division of Cellular and Molecular Toxicology, NIHS for strong support of the project, and Dr. Bruce Blumberg for critical reading of the manuscript. The project has been supported by MHLW Health Sciences Research Grants H24-Kagaku-Shitei-006, H21-Kagaku-Ippan-001, H19-Toxico-001, H18-Kagaku-Ippan-001, H15-Kagaku-002, H14-Toxico-001, and H13-Seikatsu-012.

REFERENCES

Braun, W.H., Young, J.D., Blau, G.E. and Gehring, P.J. (1977): The pharmacokinetics and metabolism of pentachlorophenol in rats. Toxicol. Appl. Pharmacol., **41**, 395-406.

Carignan, D., Désy, O. and de Campos-Lima, P.O. (2011): The dysregulation of the monocyte/macrophage effector function induced by isopropanol is mediated by the defective activation of distinct members of the AP-1 family of transcription factors. Toxicol. Sci., **125**, 144-156.

Clayton, G.D. and Clayton, F.E. (1981): Toxicology. John Wiley Sons, New York.

Damm, J., Wiegand, F., Harden, L.M., Gerstberger, R., Rummel, C. and Roth, J. (2012): Fever, sickness behavior, and expression of inflammatory genes in the hypothalamus after systemic and localized subcutaneous stimulation of rats with the Toll-like receptor 7 agonist imiquimod. Neuroscience, **201**, 166-183.

Deichman, W., Machle, W., Kitzmiller, K.V. and Thomas, G. (1942): Acute and chronic effects of pentachlorophenol and sodium pentachlorophenate upon experimental animals. J. Pharmacol. Exp. Ther., **76**, 104-117.

Dinarello, C.A. (1999): Cytokines as endogenous pyrogens. J Infect Dis., **179 Suppl. 2**, S294-S304.

Finck, B.N., Gropler, M.C., Chen, Z., Leone, T.C., Croce, M.A., Harris, T.E., Lawrence, J.C.Jr. and Kelly, D.P. (2006): Lipin 1 is an inducible amplifier of the hepatic PGC-1alpha/PPARalpha regulatory pathway. Cell. Metab., **4**, 199-210.

Gomard, T., Michaud, H.A., Tempé, D., Thiolon, K., Pelegrin, M. and Piechaczyk, M. (2010): An NF-kappaB-dependent role for JunB in the induction of proinflammatory cytokines in LPS-activated bone marrow-derived dendritic cells. PLoS One, **5**, e9585.

Hemmi, H., Kaisho, T., Takeuchi, O., Sato, S., Sanjo, H., Hoshino, K., Horiuchi, T., Tomizawa, H., Takeda, K. and Akira, S. (2002): Small anti-viral compounds activate immune cells via the TLR7 MyD88-dependent signaling pathway. Nat. Immunol., **3**, 196-200.

Jung, J., Ishida, K. and Nishihara, T. (2004): Anti-estrogenic activity of fifty chemicals evaluated by in vitro assays. Life Sci., **74**, 3065-3074.

Kanno, J., Aisaki, K., Igarashi, K., Nakatsu, N., Ono, A., Kodama, Y. and Nagao, T. (2006): "Per cell" normalization method for mRNA measurement by quantitative PCR and microarrays. BMC Genomics, **7**, 64.

Kawaguchi, M., Morohoshi, K., Saita, E., Yanagisawa, R., Watanabe, G., Takano, H., Morita, M., Imai, H., Taya, K. and Himi, T. (2008): Developmental exposure to pentachlorophenol affects the expression of thyroid hormone receptor beta1 and synapsin I in brain, resulting in thyroid function vulnerability in rats. Endocrine, **33**, 277-284.

Konishi, H., Okamoto, K., Ohmori, Y., Yoshino, H., Ohmori, H., Ashihara, M., Hirata, Y., Ohta, A., Sakamoto, H., Hada, N., Katsume, A., Kohara, M., Morikawa, K., Tsukuda, T., Shimma, N., Foster, G.R., Alazawi, W., Aoki, Y., Arisawa, M. and Sudoh, M. (2012): An orally available, small-molecule interferon inhibits viral replication. Sci. Rep., **2**, 259.

Larsen, R.V., Kirsch, L.E., Shaw, S.M., Christian, J.E. and Born, G.S. (1972): Excretion and tissue distribution of uniformly labeled 14 C-pentachlorophenol in rats. J. Pharm. Sci., **61**, 2004-2006.

Lucas, K. and Maes, M. (2013): Role of the Toll Like Receptor (TLR) Radical Cycle in Chronic Inflammation: Possible Treatments Targeting the TLR4 Pathway. Mol. Neurobiol., (in press).

NTP (1999): NTP Toxicology and Carcinogenesis Studies of Pentachlorophenol (CAS NO. 87-86-5) in F344/N Rats (Feed Studies). In: Natl Toxicol Program Tech Rep Ser), pp.1-182.

Ohnishi, T., Yoshida, T., Igarashi, A., Muroi, M. and Tanamoto, K. (2008): Effects of possible endocrine disruptors on MyD88-independent TLR4 signaling. FEMS Immunol. Med. Microbiol., **52**, 293-295.

Puigserver, P., Rhee, J., Donovan, J., Walkey, C.J., Yoon, J.C., Oriente, F., Kitamura, Y., Altomonte, J., Dong, H., Accili, D. and Spiegelman, B.M. (2003): Insulin-regulated hepatic gluconeogenesis through FOXO1-PGC-1alpha interaction. Nature, **423**, 550-555.

Sato, M., Suemori, H., Hata, N., Asagiri, M., Ogasawara, K., Nakao, K., Nakaya, T., Katsuki, M., Noguchi, S., Tanaka, N. and Taniguchi, T. (2000): Distinct and essential roles of transcription factors IRF-3 and IRF-7 in response to viruses for IFN-alpha/beta gene induction. Immunity, **13**, 539-548.

Tasaki, M., Kuroiwa, Y., Inoue, T., Hibi, D., Matsushita, K., Ishii, Y., Maruyama, S., Nohmi, T., Nishikawa, A. and Umemura, T. (2012): Oxidative DNA damage and *in vivo* mutagenicity caused by reactive oxygen species generated in the livers of p53-proficient or -deficient gpt delta mice treated with non-genotoxic hepatocarcinogens. J. Appl. Toxicol. DOI: 10.1002/jat.2807.

Zhu, B.Z. and Shan, G.Q. (2009): Potential mechanism for pentachlorophenol-induced carcinogenicity: a novel mechanism for metal-independent production of hydroxyl radicals. Chem. Res. Toxicol., **22**, 969-977.

The web site for GeneChip data

The GeneChip data of PCP are accessible at
http://www.nihs.go.jp/tox/TtgPublished.htm

The Journal of Toxicological Sciences (J. Toxicol. Sci.)
Vol.38, No.4, 619-628, 2013

Original Article

An improved dispersion method of multi-wall carbon nanotube for inhalation toxicity studies of experimental animals

Yuhji Taquahashi, Yukio Ogawa, Atsuya Takagi, Masaki Tsuji, Koichi Morita and Jun Kanno

Division of Cellular and Molecular Toxicology, Biological Safety Research Center, National Institute of Health Sciences, 1-18-1 Kamiyoga, Setagaya-ku, Tokyo 158-8501, Japan

(Received May 5, 2013; Accepted June 9, 2013)

ABSTRACT — A multi-wall carbon nanotube (MWCNT) product Mitsui MWNT-7 is a mixture of dispersed single fibers and their agglomerates/aggregates. In rodents, installation of such mixture induces inflammatory lesions triggered predominantly by the aggregates/agglomerates at the level of terminal bronchiole of the lungs. In human, however, pulmonary toxicity induced by dispersed single fibers that reached the lung alveoli is most important to assess. Therefore, a method to generate aerosol predominantly consisting of dispersed single fibers without changing their length and width is needed for inhalation studies. Here, we report a method (designated as Taquann method) to effectively remove the aggregate/agglomerates and enrich the well-dispersed singler fibers in dry state without dispersant and without changing the length and width distribution of the single fibers. This method is base on two major concept; liquid-phase fine filtration and critical point drying to avoid re-aggregation by surface tension. MWNT-7 was suspended in Tert-butyl alcohol, freeze-and-thawed, filtered by a vibrating 25 μm mesh Metallic Sieve, snap-frozen by liquid nitrogen, and vacuum-sublimated (an alternative method to carbon dioxide critical point drying). A newly designed direct injection system generated well-dispersed aerosol in an inhalation chamber. The lung of mice exposed to the aerosol contained single fibers with a length distribution similar to the original and the Taquann-treated sample. Taquann method utilizes inexpensive materials and equipments mostly found in common biological laboratories, and prepares dry powder ready to make well-dispersed aerosol. This method and the chamber with direct injection system would facilitate the inhalation toxicity studies more relevant to human exposure.

Key words: Multi-wall carbon nanotube, Dispersion, Metallic sieve, Tert-butyl alcohol, Sublimation, Critical point drying

INTRODUCTION

We previously reported that a certain make of multi-wall carbon nanotube (MWCNT) contained particles similar to asbestos fibers in size and shape, and was positive for mesotheliomagenesis in intraperitoneal injection studies using p53-heterozygous mice (Takagi *et al.*, 2008, 2012). The intraperitoneal injection study is a specialized method for the detection of mesotheliomagenic potential of inhaled fibrous materials (Pott *et al.*, 1994; Roller *et al.*, 1997; Poland *et al.*, 2008). For the assessment of general respiratory toxicity including non-cancerous endpoints, the inhalation studies are considered essential. As a surrogate for inhalation studies, pharyngeal aspiration and intratracheal spray methods are often used. However, in both methods, the suspension medium may modify the distribution and/or the toxicity of the test particles (Morimoto *et al.*, 2011; Oyabu *et al.*, 2011; Gasser *et al.*, 2012; Wang *et al.*, 2012). Dispersion methods without suspension media are reported. However, those are usually using, at least in part of the processes, rigorous sonication or mechanical milling resulting in certain degree of physiological changes in sample characteristics, such as shortening in length distribution of MWNCT (Muller *et al.*, 2005; Mitchell *et al.*, 2007; Ahn *et al.*, 2011). Changes in particle size and/or shape will also affect the nature

Correspondence: Jun Kanno (E-mail: kanno@nihs.go.jp)

and strength of toxicity of the test substances. Therefore, development of a dispersion method to generate the aerosol of concern without addition of chemicals and changes in particle dimensions is considered to be essential for the assessment of inhalation toxicity in humans.

Fibrous nanomaterial such as Mitsui MWNT-7 is a mixture of dispersed single fibers of various length and width, and their agglomerates and aggregates. When given as a mixture, the lung lesions were mainly seen as inflammatory and/or granulomatous lesions with various degree of fibrosis at the level of terminal bronchiole accompanying the aggregates and agglomerates. These lesions were considered to block and/or mask the changes induced by the single fibers that should have reached the alveolar ducts and alveoli (Warheit *et al.*, 2004; Muller *et al.*, 2005; Shvedova *et al.*, 2008; Porter *et al.*, 2009; Mercer *et al.*, 2011; Wang *et al.*, 2011). Therefore, assessment of the toxicity of single fibers needs well-dispersed sample without aggregate/agglomerate. In practical inhalation testing, the animal chamber air is rigorously agitated in order to ensure the homogeneity of aerosol in the chamber. Therefore, if the MWNT-7 as a mixture is used, the likelihood of aggregates/agglomerates reaching the nose of the animals is high. In contrast, human ambient air is less agitated; the aggregates/agglomerates may sediment away fast and dispersed single fibers may stay longer in the air to be inhaled by humans (Han *et al.*, 2008). In addition, humans have longer respiratory tract compared to rodents and may effectively filtered out aggregates/agglomerates before the air reaches the alveolar region.

Taking all into account, we concluded that it is essential to prepare a dispersed single fiber aerosol without aggregate/agglomerates, without additional chemical components, and without changes in size and shape of the single fiber component for the rodent inhalation studies in order to predict human inhalation toxicity. To date, one dispersion method is reported, i.e. the filtration system. Filtration by a sieve with its pore size smaller than the size of aggregates/agglomerate will not affect the size distribution of the single fibers (Kasai *et al.*, 2013). However, filtration in gaseous phase turns out to be ineffective in terms of yield of the filtrate. Filtration in liquid phase is much efficient (Mercer *et al.*, 2008; Tsuda, personal communication). However, in our experience, the difficulty is found in avoiding re-aggregation during the process of drying; the surface tension. To solve this problem, here we report a new improved dispersion method consisting of a combination of aqueous filtering and the concept of a drying method used for scanning electron microscopic (SEM) samples; the critical point drying.

MATERIALS AND METHODS

MWCNT, reagent and equipments

MWCNT (Mitsui MWNT-7) was kindly donated by Mitsui & Co., Ltd., Tokyo, Japan for use in toxicity studies (Takagi *et al.*, 2008). Tert-butanol (TB) of guaranteed reagent grade was used (CAS: 75-65-0, Kanto Chemical Co., Inc., Tokyo, Japan). Metallic Sieve (pore size 25 μm mesh, Seishin Enterprise Co., LTD., Tokyo, Japan) was used for filtration. Miniature coin type vibration motors used in cellular phones (Model FM34F, T.C.P. Co, Tokyo Japan; 13,000 rpm 1.8m²/sec) are attached to the extended filler rim (5cm in depth, custom-made, Seishin Enterprise Co., LTD.) of the metallic sieve (cf. Fig. 1c) to gain high yield of filtrate. Chemistry diaphragm pumps and pumping systems (Model; MD4C NT+AK+EK, Vacuubrand, Wertheim, Germany) was used for sublimation of the frozen TB suspension and recovery of TB. Glass wares such as funnel, filtering bottle, trap bottle and silicon stoppers (Sansyo Co., Ltd., Tokyo, Japan), laboratory bottles (Pyrex®, Asahi Glass Co. Ltd., Tokyo, Japan), were used.

Dispersion method ("Taquann" method)

An outline flowchart is shown in Fig. 1. TB (melting point 25.69°C) was heated up to 60°C by a mantle heater (Sibata Scientific Technology Ltd., Saitama, Japan). It is advised not to use water bath; TB is highly hygroscopic and becomes difficult to freeze and sublimate. A volume of 200 ml of TB and 0.2 g of MWCNT were transferred to a 500 ml laboratory bottle and agitated to make crude suspension. The bottle was put into an ice bath, occasionally shaken by hand, until the suspension starts to freeze and becomes sherbet-like half frozen state and kneaded by a stainless steel spatula until it becomes evenly gray without clear crystals of TB (Fig. 1a), and then kept overnight at -25°C. To the frozen suspension, 500 ml of TB pre-heated to 60°C, was added, capped and shaken hard until the liquefied suspension becomes evenly dark brown to gray in color (Fig. 1b). The bottle was further heated up to 60°C by a mantle heater and the suspension was immediately applied to vibrating metal sieve for filtration (Fig. 1c). The filtrate was collected through a funnel into a 1,000 ml laboratory bottle. Immediately after the filtration, approximately 1,500 ml of liquid nitrogen was poured onto the filtrate in the bottle to snap freeze the suspension (Fig. 1d). Then, the bottle was connected to the pumping system and vacuumed until TB was totally sublimated; leaving dispersed MWCNT (T-CNT for Taquann-treated MWCNT) in the bottle. The MWCNT was collected by a cyclone-suction bottle using conduc-

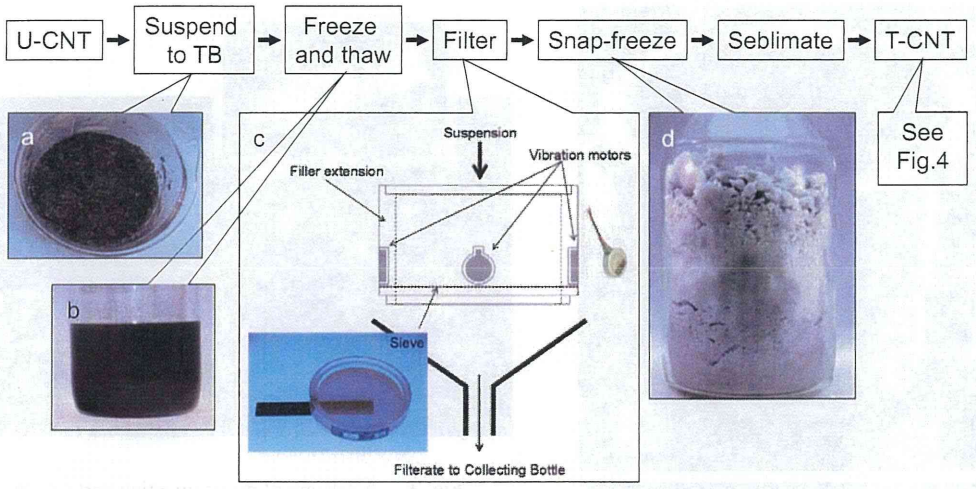

Fig. 1. Outline flowchart of the Taquann method. a) Half-frozen sherbet-like suspension of MWNT-7 kneaded (beaker was used for demonstration). b) Well-shaken liquefied suspension after adding 60°C TB (beaker was used for demonstration). c), Photograph of the sieve on a backlight box with a scale underneath (left inset), vibration motor (right inset), and a diagram of the filter unit with a filler extension and vibration motors. d) Snap-frozen filtrate.

tive silicon and aluminum tubing. In order to make a precise aliquot, a measured amount the collected T-CNT was resuspended to TB, and the suspension was aliquoted into proper containers, in this study into the newly designed cylindrical cartridge case (cf. Fig. 3), snap-frozen, and sublimated.

Aerosol generation system

An originally designed 105 L main exposure chamber (capacity of 16 mice per chamber), with a disposable electrostatic-free plastic bag inside, was prepared (Fig. 2, patent pending, manufactured by Sibata Scientific Technology Ltd.). Onto the plastic disposable top plate, a 20 L subchamber was connected with a 5 cm-diameter 10 cm long connecting pipe. To the subchamber, an injection port was connected, to which a newly designed cylindrical cartridge (manufactured by Sibata Scientific Technology Ltd.) containing dispersed T-CNT is loaded. The cartridge has a slide-valve air inlet at its base and four ejection holes at its top opening towards the subchamber lumen. The compressed air (0.8 M pascal) was injected five times with 0.2 sec duration and 10 sec interval to empty the T-CNT into the subchamber (Fig. 3). The carrier air flow from the subcamber to the main chamber was 15 L/min. Twenty-one cartridges were prepared for a two-hr exposure experiment, loading first two in 1 min for an initial boost and then one in every 6 min, resulting in generation of saw-tooth concentration wave with an average of 1.3 mg/m^3 (250 μg/cartridge) and 2.8 mg/m^3 (500 μg/cartridge).

Twelve C57BL/6NCrSlc male mice (SLC, Inc., Shizuoka, Japan), 10~11 weeks old, body weight of 23.8~30.8 g were placed in the cage suspended from the top plate of the inhalation chamber and exposed to 1 mg/m^3 of T-CNT for 2 hr a day for 5 days, lungs (excluding primary bronchi) were sampled and subjected to characterization of deposited fibers (see below).

The animal study was conducted in accordance with the Guidance for Animal Studies of the National Institute of Health Sciences under Institutional approval.

Real time particle counting and weight measurement

An optical particle counter (OPC) with a nominal detection limit of 300 nm (OPC-110GT, Sibata Scientific Technology Ltd.) and a condensation particle counter (CPC) with a nominal detection limit of 2.5 nm (ultrafine condensation particle counter 3776, Trust Science Innovation, MN, USA) were connected to the main chamber with a sample flow of 2.83 L (0.1cf) /min and 0.3 L/min respectively. The mass concentration of the chamber aerosol was calculated from the weight increase of polytetrafluoroethylene-glass fiber filter (Model T60A20, φ55mm, Tokyo Dylec Corp, Tokyo, Japan) after filtering the chamber aerosol by an Asbestos sampling pump (AIP-105, Sibata Scientific Technology Ltd.) at a rate of 1.5 L/min for 120 min (total of 180 L). Filter weight was measured by a microbalance (XP26V,

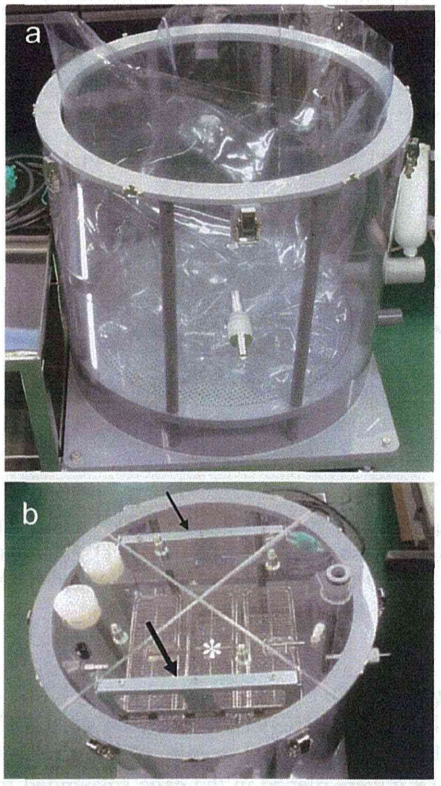

Fig. 2. Newly designed original inhalation chamber. a) Outer chamber and inner bag before top plate is in place. During operation, the space between the outer chamber and inner bag is negatively pressured to inflate the inner bag. B) Disposable top plate with tubing holes are placed on the chamber. The animal cages for 16 mice (asterisk) are suspended from the top place by a pair of hanger arms (arrows) (photo was taken without inner bag for better demonstration).

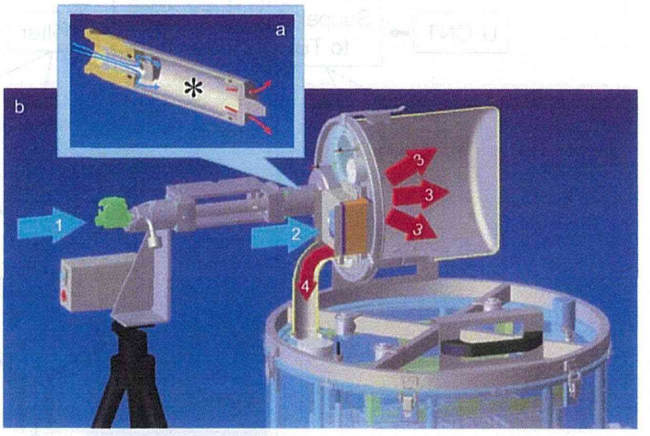

Fig. 3. A scheme of direct injection aerosol generation system. a) Upper inset shows the cut section of the injection cartridge (capacity; 23.5 ml). A slide valve opens when the cartridge is loaded to the subchamber. A measured amount of dispersed MWCNT is preloaded inside the cartridge shown in asterisk. b) Compressed air (Blue arrow 1) blows out the MWCNT through four small outlets of the cartridge into the subchamber (red arrows 3), where main flow air from the HEPA filtered inlet (blue arrow 2) mixes in. The air with the aerosol goes down the connection pipe to the main chamber (red arrow 4).

Mettler Toledo).

Characterization of the dispersed MWCNT

The T-CNT in TB suspension was mounted on a slide glass and observed under a light microscope using a pair of polarizing filters. Untreated MWCNT (U-CNT) from the bulk, 200 mg, was dispersed in to 500 ml of TB and sonicated for 30 min at 40W, 3.4 kHz (SU-3TH, Sibata Scientific Technology Ltd.) and observed.

A weight-measured aliquot of T-CNT was re-suspended, blotted on a Anopore™ Inorganic Aluminum Oxide Membrane Filters (Whatman GmbH, Dassel GE Healthcare, Hahnestrasse, Germany, pore size; 0.02 μm, φ13 mm, Anodisc 13) or a cellulose acetate/nitrocellulose membrane filter (MFTM- Millipore Membrane filters, 0.025 μm, φ13 mm, Merck Millipore, Billerica, MA, USA) and observed with a scanning electron microscope (SEM).

From the main chamber, the aerosol was collected at a rate of 5 L/min for 3 min on a Anopore™ Inorganic Aluminum Oxide Membrane Filters (Whatman GmbH, pore size; 0.1 um, Anodisc 25) joined to asbestos sampling pump (AIP-105, Sibata, Scientific Technology Ltd.). A scanning electron microscope (SEM) (VE-9800, Keyense Co., LTD., Osaka, Japan) was used for monitoring the details of the samples on the slide glasses and on the Anodiscs after osmium coating (HPC-1SW, Vacuum Device Inc., Ibaraki, Japan).

From the exposed mouse, lung lobes are collected and treated with lysis solution composed of 5 w/v% potassium hydroxide (Super Special Grade, Wako Pure Chemical Industries, Ltd., Osaka, Japan), 0.1w/v% Sodium dodecyl sulfate (SDS, for Biochemistry, Wako Pure Chemical Industries, Ltd.), 0.1 w/v% Ethylenediamine-N,N,N',N'-tetraacetic acid disodium salt dehydrate (EDTA 2Na, Dojindo laboratories, Kumamoto, Japan) and 2w/v% ascorbic acid (Super Special Grade, Wako Pure Chemical Industries, Ltd.) in ultra-pure water, dissolved at 80°C (Fig. 10b). Lung samples (approx. 200 mg) and 1.8 ml of

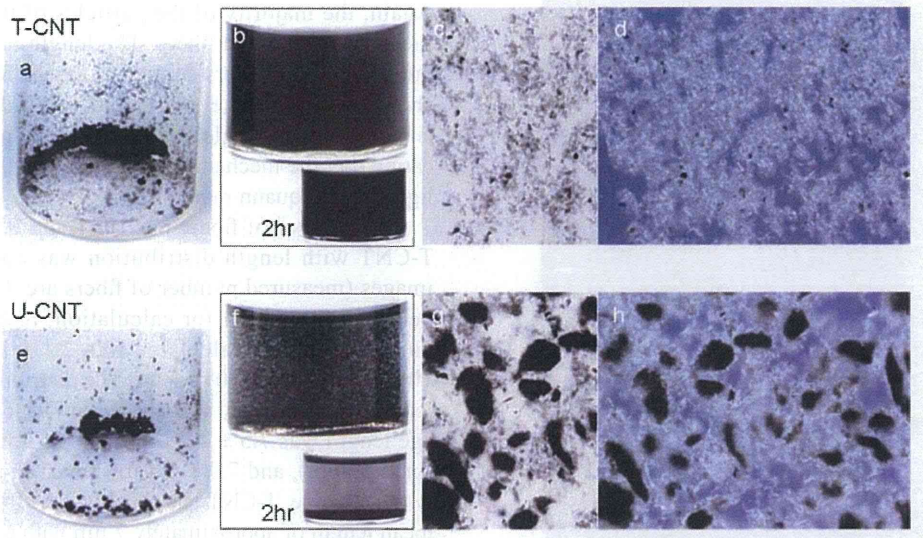

Fig. 4. Taquann-treated carbon nanotube (T-CNT) and untreated bulk carbon nanotube (U-CNT). a) final fine and dry powder of Taquann-treated MWCNT. b) Resuspended T-CNT to TB and placed for 5 min and 2 hr; T-CNT suspension is stable, compared to U-CNT, c) light microscopic view of the resuspended T-CNT on a slide glass, and d) under polarized light. e) course powder of U-CNT, f) Resuspended U-CNT to TB and placed for 5 min and 2 hr. g) light microscopic view of the resuspended U-CNT on a slide glass, and d) under polarized light. (diameter of the vials in a), b), e) and f) is 2.3 cm)

lysis solution in a centrifuge tube (DNA LoBindid tube 2.0 ml, Eppendorf, Hamburg, Germany) was incubated at 80°C for approx. 24 hr in an oven (HV-100, Funakoshi Co., Ltd., Tokyo, Japan), centrifuged at 20,000 g for 1 hr at 25°C (MX-207, Tomy Seiko Co., Ltd., Tokyo, Japan), and the pellet containing MWCNTs and SDS crystals was recovered. 1.8 ml of 70% ethanol was added to the tube and incubated at 80°C for 30 min to dissolve SDS crystals and centrifuged at 20,000 g for 1 hr at 25°C. 100 µl of 1w/w% Triton®X-100 (MP Biomedicals, Inc., Solon, OH, USA) was added to the pellet and dispersed by pipetting. One microliter of the suspension was placed on an inorganic aluminum oxide membrane filter (Anodisc 13, 0.02 µm φ13mm, Whatman GmbH) or the cellulose acetate/nitrocellulose membrane filter and filtrated on a funnel shape glass filter (SANSYO Co., LTD., Tokyo, Japan). The filter was dried at room temperature and osmium coated for SEM. For a reference of extraction efficiency, lung sample from untreated mouse was spiked with 1 µg T-CNT and measured alongside.

Lung tissue from eight mice were fixed with buffered 10% formalin (four with and four without inflation), paraffin embedded and processed routinely for H&E stained histology slides, and observed under a light microscope with or without polarizing filters (Olympus BX50 microscope with DP-70 image system, Olympus Corporation, Tokyo, Japan).

RESULTS

Characteristics of "Taquann"-dispersed MWCNT

Macroscopic and light microscopic views of the final product, the dried MWCNT after sublimation, i.e. "Taquann"-dispersed MWCNT (T-CNT) and, for comparison, untreated MWCNT from the bulk (U-CNT) are shown in Fig. 4. The powder of T-CNT is finer compared to U-CNT (Fig. 4a). The T-CNT resuspended very well to TB (Fig. 4b) and other solvents including 0.1 w/v% Sodium dodecyl sulfite and 0.1 w/v% Sodium dodecylbenzene sulfonate (not shown). Light microscopically, the resuspended T-CNT consists mostly of dispersed single fibers with smaller numbers of small aggregates corresponding to the mesh size of the metal sieve (Figs. 4c, 4d), whereas U-CNT was a mixture of large aggregates/agglomerates and single fibers among them (Figs. 4g, 4h). The T-CNT fibers slowly precipitated in the medium (cf. Figs. 4b and f), and are easily resuspended by gentle agitation. The yield of the T-CNT was approximately 5% of the U-CNT in weight. Re-filtration of the residue on the sieve resulted in negligible yield. The low power SEM views of the TB-resuspended T-CNT and U-CNT are shown in Fig. 5.

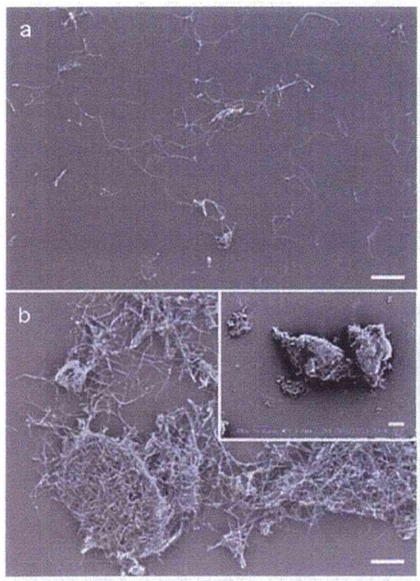

Fig. 5. Scanning electron microscopy of T-CNT and U-CNT resuspended in TB. a) T-CNT consists mainly of dispersed single fibers with few small aggregates/agglomerates smaller than the mesh size of the sieve, SEM x 1,000. b) U-CNT showing mixture of single fibers and large aggregates/agglomerates, SEM x 1,000. The length and width distribution of the single fibers of T-CNT were virtually identical to those of U-CNT. Inset; Lower power view to demonstrate larger aggregates/agglomerates measuring up to 300 μm in major axis SEM x 400. (scale bars are 10 μm)

Again, the majority of the particles of the T-CNT were the dispersed single fibers. The length and width distribution of single fibers counted on these SEM images are shown in Fig. 6. The length and width distribution was similar between single fibers of T-CNT and U-CNT, indicating that the mechanical shortening of the fibers is negligible for Taquann method.

The number of fibers per 10, 1 and 0.1 μg weight of T-CNT with length distribution was counted on SEM images (measured number of fibers are 959, 246, and 45 per designated area for calculation, respectively). The number of fibers calculated was 2.1 x 10^7/10 μg 4.1 x 10^6/1 μg and 3.3 x 10^5/0.1 μg. The distribution of the fiber length was similar to that shown in Fig. 6a, and the average length was 7.5 ± 4.7 μm (max 34 μm), 8.7 ± 6.4 μm (max 42 μm), and 7.0 ± 5.4 μm (max 26 μm) respectively. As a whole, T-CNT has roughly 3 x 10^6 fibers per 1 μg, mean length of approximately 7 μm with a length range up to 50 μm with a median of approximately 6.5 μm.

"Taquann"-dispersed MWCNT in the inhalation chamber

The T-CNT aerosol generated at an average concentration of 1 mg/m³ was sampled on the Anodisc and observed by a SEM (Fig. 7). The aerosol was composed mainly of well-dispersed single fibers and some small tangles of fibers admixed with a relatively small amount of non-fibrous particles.

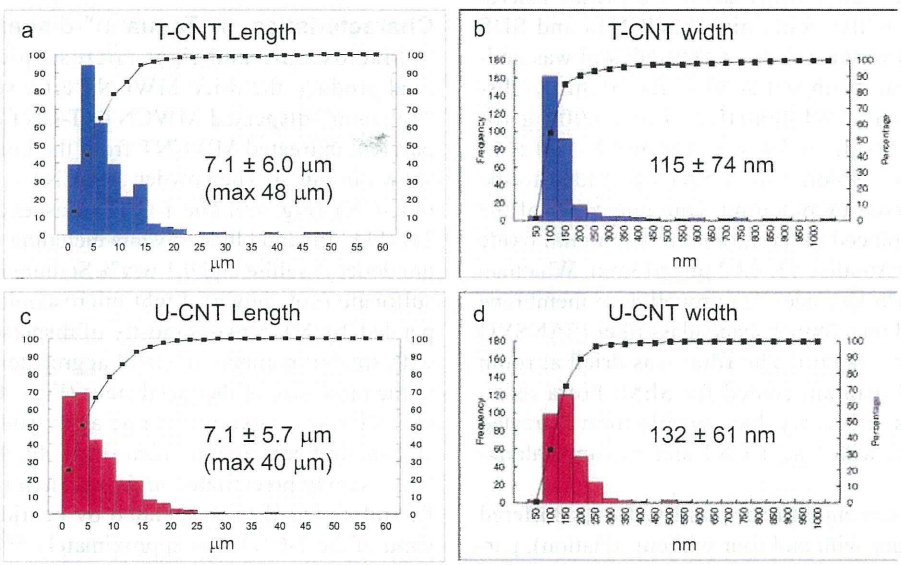

Fig. 6. Length and width of single fibers in T-CNT and U-CNT (measured by SEM on TB-resuspended samples). a) Length distribution and b) width distribution of Taquann-treated MWNT-7. c) Length distribution and d) width distribution of single fibers in the mildly sonicated suspension of the bulk MWNT-7 (mean ± s.d., n = 304 each).

Table 1. Aerosol particle count by optical particle counter (OPC) and condensation particle counter (CPC).

	Date of measurement	2013/4/29	2013/5/1	2013/5/3
Equipment	Mass concentration (mg/m³)	1.25	1.25	1.38
OPC	Average cpm* (/L) ± s.d.	627,096 ± 145,399	781,973 ± 138,610	821,272 ± 114,278
	K-value (mg/m³/cpm)	1.99×10^{-9}	1.60×10^{-9}	1.68×10^{-9}
CPC	Average cpm (/L) ± s.d.	859,692 ± 171,858	1,228,545 ± 223,371	1,317,873 ± 217,990
	K-value(mg/m³/cpm)	1.45×10^{-9}	1.02×10^{-9}	1.05×10^{-9}

*count per minute

Fig. 7. T-CNT aerosol at a concentration of 1 mg/m³ in the main chamber was collected on the Anodisc filter (5 L/min for 3 min). SEM x 1,000. (scale bar is 10 μm)

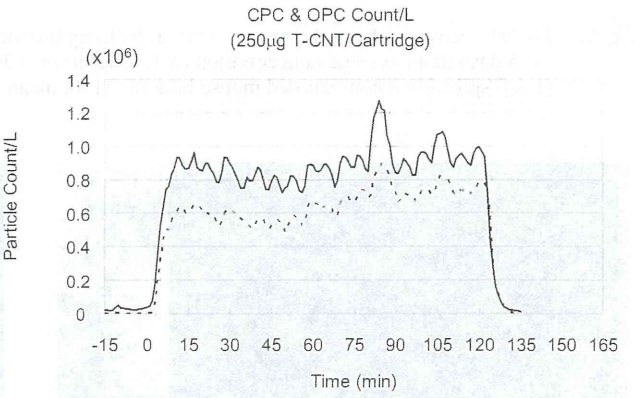

Fig. 8. A real time data from condensation particle counter (CPC, solid line) and optical particle counter (OPC, dotted line) from an inhalation chamber injected with T-CNT (250 μg/cartridge) from 0 min to 120 min with an average injection interval of 6 min (for detail see text).

From the amount of weight increase of polytetrafluoroethylene-glass fiber filter after sampling the chamber aerosol, the weight of aerosol per m³ of the chamber air (weight concentration) was calculated as approximately 1.3 mg/m³ (average of three measurements shown in Table 1). At the same time, the particle counts per m³ given by OPC and CPC were recorded (Fig. 8), and the K-value (mg/particle count in m³) was calculated (Table 1).

K-value (mg/m³/cpm), i.e. the weight concentration (mg/m³) divided by OPC or CPC count per minute (cpm) is often used as an indicator of the status of dispersion. Three measurements conducted with a few days' interval showed that not only the K-values itself but also the values used to calculate it were fairly stable over a period of days.

The length distribution of the T-CNT recovered from the lungs of two mice exposed in the whole body inhalation chamber 2 hr a day for 5 days at an average concentration of 1.8 mg/m³ of T-CNT are shown in Fig. 9 along with the data from the spiked lung tissue sample. The average length were 8.4 ± 5.0 μm and 8.3 ± 4.9 μm (Figs. 9a, 9b), comparable to that of the T-CNT in spiked lung tissue sample; 9.5 ± 5.2 μm (Fig. 9c) (width was qualitatively not different, data not shown). The total numbers of the fibers recovered were 5.1×10^6 and 3.2×10^6 from the inhaled lungs and 1.6×10^6 from the spiked lung; the weight of T-CNT deposited in the lung after 2 hr x 5 days of inhalation was roughly calculated as 3 μg/lung.

The fibers recovered from one of the mice were observed with SEM (Fig. 10a). Dispersed single fibers were found and some of which are longer that 20 μm (cf. Fig. 9). It was noted that EDTA and ascorbic acid in the lysis solution were effective in removing the debris from the SEM sample (Fig. 10b).

Histologically, the CNTs were found to distribute from bronchial lumen to peripheral alveolar spaces. In the bronchial lumen, the fibers were trapped in the bronchial mucus, either as single fibers or as loose aggregates

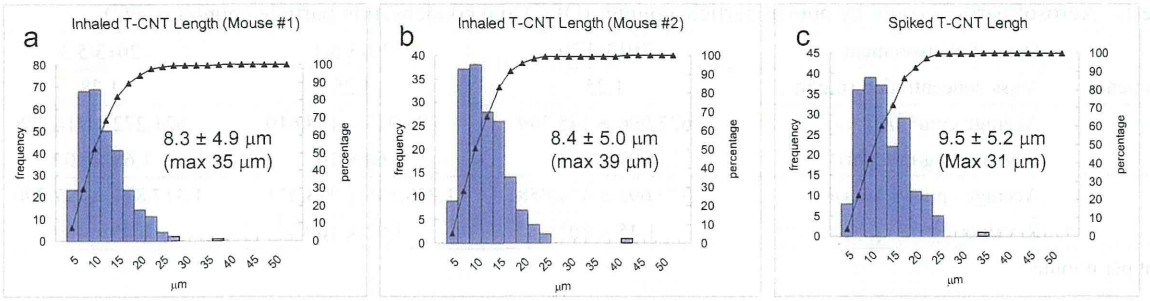

Fig. 9. T-CNT recovered from the mouse lung. a, b) Length distribution of T-CNT in the lung of two mice exposed 2 hr a day for 5 days at an average concentration of 1.8 mg/m³ (n = 306 and 166 each, mean ± s.d). c) Length distribution of T-CNT (1 μg) spiked to a non-exposed mouse lung (n = 198, mean ± s.d).

Fig. 10. T-CNT recovered from the mouse lung. a) SEM of the sediment of the dissolved lung of a mouse exposed to T-CNT in an inhalation chamber 2 hr a day for 5 days, x 2,000. Long and short single fibers are shown to be inhaled (treated with solution containing EDTA and ascorbic acid). b) SEM of a same sample treated without EDTA and ascorbic. The debris covering the fibers is considered to be iron-based amorphous substances soluble to EDTA, x 2,000. Ascorbic acid was found to be effective in keeping iron ions to be bivalent (ferrous) and soluble. (scale bars are 10 μm)

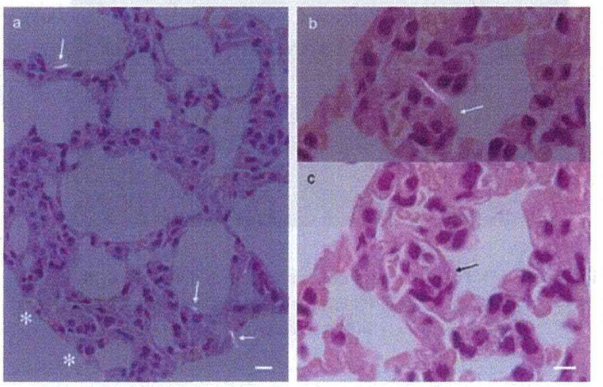

Fig. 11. a) A polarized microscopic view of the alveolar region of a lung exposed to 1 mg/m³ of T-CNT for 2 hr a day for 5 days. Arrows indicate single T-CNTs deposited in alveolar spaces phagocytized by alveolar macrophages. Asterisks indicates visceral pleural. (scale bar 10 μm) b,c) Another portion of alveolar region with a tadpole-shaped alveolar macrophage containing single long CNT in its cytoplasm shown in plain and polarized view. The lungs shown here are not inflated with formalin at fixation in order to avoid replacement of the CNTs. (scale bar 5 μm)

without inflammatory or granulomatous response, morphologically interpretable as a view of expectoration by the ciliary movement of the bronchial epithelium. There were no dense aggregates/agglomerates in the lungs so far as examined. In the peripheral alveolar space, single fibers are found phagocytized in alveolar macrophages as shown in Fig. 11. There were only mild inflammatory reactions such as neutrophilic migration against fibers in mucous blanket of the bronchial/bronchiolar segments and fibers in the alveolar space.

DISCUSSION

The MWCNT treated with the "Taquann" method (T-CNT) consisted of highly dispersed single fibers with marked reduction of aggregates/agglomerates, both in the aerosol and in the resuspended solution. The length and width distribution of the single fibers were not different between the T-CNT and the original U-CNT, indicating that this method is physically mild to the sample and does not shorten the fibers.

The Taquann method consists of two major steps, the

efficient filtration in liquid phase and the idea of critical point drying in order to prevent re-aggregation of the fibers by surface tension during drying. The latter step was inspired by the drying method for SEM samples. TB-sublimation technique used in this study is an alternative method used for SEM samples as well. Our trial-and-error added a few innovations such as gentle kneading of half-frozen TB suspension and a freeze-and-thaw process for a better dispersion (visible differences in fineness of suspension, data not shown), and vibration of the sieve for a faster and better yield of filtrate (approximately 7 fold increase in half the time). This Taquann method does not use high power sonication or other strong mechanical shearing, so that the length distribution of the single fibers did not change. The equipments and reagents used here are mostly available at regular biological or chemical laboratories. The new aerosol generating system by the direct injection of T-CNT had successfully generated highly dispersed aerosol of MWNT-7 and an exposure study confirmed the inhalation of MWNT-7 single fibers in mouse lung down to the peripheral alveolar spaces. In this condition, i.e. five consequtive days of 2 hr exposure, histologically, there were only mild neutrophilic infiltration. A long-term follow up study is underway.

It is highly plausible that the Taquann method can be applied to other types of particles as long as they are not soluble to TB (additional study in preparation). Well-dispersed samples generated by the Taquann method, together with the direct injection and the small scale inhalation chamber system, would facilitate the inhalation toxicity studies more relevant to human exposure not only at the big facilities but also at the small scaled laboratories.

Finally, this dispersion method may also be useful for industries where difficulty in dispersion of nanoparticles was a limiting process in developing new products. For a large scale manufacturing, carbon dioxide critical point drying may be suitable than TB sublimation.

ACKNOWLEDGMENT

The authors thank Dr. Hiroyuki Tsuda for introducing the metal sieve for liquid phase filtration. This study is supported by the Health Sciences Research Grants H21-kagaku-ippan-008, H23-kagaku-ippan-005 and H24-kagaku-shitei-009 from the Ministry of Health, Labour and Welfare, Japan.

REFERENCES

Ahn, K.H., Kim, S.M. and Yu, I.J. (2011): Multi-walled carbon nanotube (MWCNT) dispersion and aerosolization with hot water atomization without addition of any surfactant. Saf. Health Work., **2**, 65-69.

Gasser, M., Wick, P., Clift, M.J., Blank, F., Diener, L., Yan, B., Gehr, P., Krug, H.F. and Rothen-Rutishauser, B. (2012): Pulmonary surfactant coating of multi-walled carbon nanotubes (MWCNTs) influences their oxidative and pro-inflammatory potential in vitro. Part Fibre Toxicol., **9**, 17.

Han, J.H., Lee, E.J., Lee, J.H., So, K.P., Lee, Y.H., Bae, G.N., Lee, S.B., Ji, J.H., Cho, M.H. and Yu, I.J. (2008): Monitoring multiwalled carbon nanotube exposure in carbon nanotube research facility. Inhal. Toxicol., **20**, 741-749.

Kasai, T., Gotoh, K., Nishizawa, T., Sasaki, T., Katagiri, T., Umeda, Y., Toya, T. and Fukushima, S. (2013): Development of a new multi-walled carbon nanotube (MWCNT) aerosol generation and exposure system and confirmation of suitability for conducting a single-exposure inhalation study of MWCNT in rats. Nanotoxicology, (in press).

Mercer, R.R., Hubbs, A.F., Scabilloni, J.F., Wang, L., Battelli, L.A., Friend, S., Castranova, V. and Porter, D.W. (2011): Pulmonary fibrotic response to aspiration of multi-walled carbon nanotubes. Part Fibre. Toxicol., **8**, 21.

Mercer, R.R., Scabilloni, J., Wang, L., Kisin, E., Murray, A.R., Schwegler-Berry, D., Shvedova, A.A. and Castranova, V. (2008): Alteration of deposition pattern and pulmonary response as a result of improved dispersion of aspirated single-walled carbon nanotubes in a mouse model. Am. J. Physiol. Lung Cell. Mol. Physiol., **294**, L87-97.

Mitchell, L.A., Gao, J., Wal, R.V., Gigliotti, A., Burchiel, S.W. and McDonald, J.D. (2007): Pulmonary and systemic immune response to inhaled multiwalled carbon nanotubes. Toxicol. Sci., **100**, 203-214.

Morimoto, Y., Hirohashi, M., Ogami, A., Oyabu, T., Myojo, T., Todoroki, M., Yamamoto, M., Hashiba, M., Mizuguchi, Y., Lee, B.W., Kuroda, E., Shimada, M., Wang, W.N., Yamamoto, K., Fujita, K., Endoh, S., Uchida, K., Kobayashi, N., Mizuno, K., Inada, M., Tao, H., Nakazato, T., Nakanishi, J. and Tanaka, I. (2011): Pulmonary toxicity of well-dispersed multi-wall carbon nanotubes following inhalation and intratracheal instillation. Nanotoxicology, **6**, 587-599.

Muller, J., Huaux, F., Moreau, N., Misson, P., Heilier, J.F., Delos, M., Arras, M., Fonseca, A., Nagy, J.B. and Lison, D. (2005): Respiratory toxicity of multi-wall carbon nanotubes. Toxicol. Appl. Pharmacol., **207**, 221-231.

Oyabu, T., Myojo, T., Morimoto, Y., Ogami, A., Hirohashi, M., Yamamoto, M., Todoroki, M., Mizuguchi, Y., Hashiba, M., Lee, B.W., Shimada, M., Wang, W.N., Uchida, K., Endoh, S., Kobayashi, N., Yamamoto, K., Fujita, K., Mizuno, K., Inada, M., Nakazato, T., Nakanishi, J. and Tanaka, I. (2011): Biopersistence of inhaled MWCNT in rat lungs in a 4-week well-characterized exposure. Inhal. Toxicol., **23**, 784-791.

Poland, C.A., Duffin, R., Kinloch, I., Maynard, A., Wallace, W.A., Seaton, A., Stone, V., Brown, S., Macnee, W. and Donaldson, K. (2008): Carbon nanotubes introduced into the abdominal cavity of mice show asbestos-like pathogenicity in a pilot study. Nat Nanotechnol., **3**, 423-428.

Porter, D.W., Hubbs, A.F., Mercer, R.R., Wu, N., Wolfarth, M.G., Sriram, K., Leonard, S., Battelli, L., Schwegler-Berry, D.,

Friend, S., Andrew, M., Chen, B.T., Tsuruoka, S., Endo, M. and Castranova, V. (2009): Mouse pulmonary dose- and time course-responses induced by exposure to multi-walled carbon nanotubes. Toxicology, **269**, 136-147.

Pott, F., Roller, M., Kamino, K. and Bellmann, B. (1994): Significance of durability of mineral fibers for their toxicity and carcinogenic potency in the abdominal cavity of rats in comparison with the low sensitivity of inhalation studies. Environ. Health Perspect., **102 Suppl. 5**, 145-150.

Roller, M., Pott, F., Kamino, K., Althoff, G.H. and Bellmann, B. (1997): Dose-response relationship of fibrous dusts in intraperitoneal studies. Environ. Health Perspect., **105 Suppl. 5**, 1253-1256.

Shvedova, A.A., Kisin, E., Murray, A.R., Johnson, V.J., Gorelik, O., Arepalli, S., Hubbs, A.F., Mercer, R.R., Keohavong, P., Sussman, N., Jin, J., Yin, J., Stone, S., Chen, B.T., Deye, G., Maynard, A., Castranova, V., Baron, P.A. and Kagan, V.E. (2008): Inhalation vs. aspiration of single-walled carbon nanotubes in C57BL/6 mice: inflammation, fibrosis, oxidative stress, and mutagenesis. Am. J. Physiol. Lung Cell. Mol. Physiol., **295**, L552-565.

Takagi, A., Hirose, A., Futakuchi, M., Tsuda, H. and Kanno, J. (2012): Dose-dependent mesothelioma induction by intraperitoneal administration of multi-wall carbon nanotubes in p53 heterozygous mice. Cancer Sci., **103**, 1440-1444.

Takagi, A., Hirose, A., Nishimura, T., Fukumori, N., Ogata, A., Ohashi, N., Kitajima, S. and Kanno, J. (2008): Induction of mesothelioma in p53+/- mouse by intraperitoneal application of multi-wall carbon nanotube. J. Toxicol. Sci., **33**, 105-116.

Wang, X.. Katwa, P., Podila, R., Chen, P., Ke, P.C., Rao, A.M., Walters, D.M., Wingard, C.J. and Brown, J.M. (2011): Multi-walled carbon nanotube instillation impairs pulmonary function in C57BL/6 mice. Part Fibre. Toxicol., **8**, 24.

Wang, X., Xia, T., Duch, M.C., Ji, Z., Zhang, H., Li, R., Sun, B., Lin, S., Meng, H., Liao, Y.P., Wang, M., Song, T.B., Yang, Y., Hersam, M.C. and Nel, A.E. (2012): Pluronic F108 coating decreases the lung fibrosis potential of multiwall carbon nanotubes by reducing lysosomal injury. Nano Lett., **12**, 3050-3061.

Warheit, D.B., Laurence, B.R., Reed, K.L., Roach, D.H., Reynolds, G.A. and Webb, T.R. (2004): Comparative pulmonary toxicity assessment of single-wall carbon nanotubes in rats. Toxicol. Sci., **77**, 117-125.

Xu, J., Futakuchi, M., Shimizu, H., Alexander, D.B., Yanagihara, K., Fukamachi, K., Suzui, M., Kanno, J., Hirose, A., Ogata, A., Sakamoto, Y., Nakae, D., Omori, T. and Tsuda, H. (2012): Multi-walled carbon nanotubes translocate into the pleural cavity and induce visceral mesothelial proliferation in rats. Cancer Sci., **103**, 2045-2050.

Human Immunology 74 (2013) 395–401

Contents lists available at SciVerse ScienceDirect

journal homepage: www.elsevier.com/locate/humimm

Differential effects of a common splice site polymorphism on the generation of *OAS1* variants in human bronchial epithelial cells

Satoshi Noguchi [a,b], Emi Hamano [a,b], Ikumi Matsushita [a], Minako Hijikata [a], Hideyuki Ito [c], Takahide Nagase [b], Naoto Keicho [a,*]

[a] Department of Respiratory Diseases, Research Institute, National Center for Global Health and Medicine, Tokyo 162-8655, Japan
[b] Department of Respiratory Medicine, University of Tokyo Hospital, Tokyo 113-0033, Japan
[c] Department of Thoracic Surgery, National Center for Global Health and Medicine, Tokyo 162-8655, Japan

ARTICLE INFO

Article history:
Received 5 June 2012
Accepted 27 November 2012
Available online 5 December 2012

ABSTRACT

The 2′,5′-oligoadenylate synthetase 1 (*OAS1*) is one of the major interferon-inducible proteins and a critical component of the host defense system against viral infection. A single nucleotide polymorphism (SNP), rs10774671, presumably responsible for alternate splicing of this gene, has frequently been associated with a variety of viral diseases, including emerging respiratory infections. We investigated the SNP-dependent expression of *OAS1* variants in primary cultured human bronchial epithelial cells. Total RNA was subjected to real-time RT-PCR with specific primer sets designed to amplify each transcript variant. We found that the p46 transcript was mainly expressed in cells with the GG genotype, whereas the p42 transcript was highly expressed, and the p44a (alternate exon in intron 5), p48, and p52 transcripts were expressed to a lesser extent, in cells with the AA genotype. Immunoblot analysis revealed that the p46 isoform and a smaller amount of the p42 isoform were present in cells with the GG genotype, whereas only the p42 isoform was clearly observed in cells with the AA genotype. Cellular DNA fragmentation induced by neutrophil elastase was more preferentially found in cells with the AA genotype. Thus, our findings provide insights into the potential role of *OAS1* polymorphisms in respiratory infection.

1. Introduction

Innate immune responses are the first line of defenses against viruses. When viral infection is detected by pattern recognition receptors, infected cells produce type I (α and β) and type III (λ) interferons (IFNs) [1]. Binding of IFNs to their specific receptors leads to the induction of more than 300 IFN-stimulated genes, including *OAS1*, which encodes the enzyme 2′,5′-oligoadenylate synthetase 1 (*OAS1*) [2]. Typically, OAS1 is activated by the binding of double-stranded RNA and catalyzes the oligomerization of ATP into 2′,5′-linked oligoadenylates (2-5A) [3,4]. These 2-5A, in turn, bind to latent ribonuclease L (RNase L), which then dimerizes into an active form. The activated RNase L degrades viral and cellular single-stranded RNA [5].

Eight isoforms of *OAS1* with different carboxyl (C)-terminal amino acid sequences have been registered in the public database. Among them, the p42, p46, and p48 isoforms were found earlier and their functions have been studied well [6]. The C-terminal tail of the p48 isoform has a unique Bcl-2 homology-3 (BH3) domain, which interacts with anti-apoptotic proteins of the Bcl-2 family [7]. Therefore, the p48 isoform may have dual functions, potentiating apoptosis through the BH3 domain as well as activating RNase L via the classical anti-viral pathway [8,9].

Bonnevie–Nielsen et al. have demonstrated that an A/G single nucleotide polymorphism (SNP) at the splice acceptor site of exon 6 (rs10774671) contributes to generation of these three isoforms through alternative splicing [10]. According to their study using human lymphocytes, the G allele generates the p46 transcript, while the A allele abrogates the production of the p46 transcript and drives splicing to occur further downstream, leading to generation of the p48 and p52 transcripts.

To date, polymorphisms of *OAS1* and other immune-related genes have been reported to affect susceptibility to a variety of viral diseases [11]. In mice, a single missense mutation of the 2′,5′-oligoadenylate synthetase 1B (*Oas1b*) gene, a murine ortholog of *OAS1*, determines resistance to flaviviruses, including West Nile virus (WNV) [12,13]. In humans, the A allele of SNP rs10774671 in *OAS1* was associated with susceptibility to infection with WNV [14]. An *OAS1* SNP (rs2660) in strong linkage disequilibrium (LD)

Abbreviations: LD, linkage disequilibrium; HBE, human bronchial epithelial cells; SARS, severe acute respiratory syndrome; NE, neutrophil elastase.

* Corresponding author. Address: Department of Respiratory Diseases, Research Institute, National Center for Global Health and Medicine, 1-21-1 Toyama, Shinjuku-ku, Tokyo 162-8655, Japan. Fax: +81 3 3202 7364.
E-mail address: nkeicho-tky@umin.ac.jp (N. Keicho).

0198-8859/$36.00 - see front matter © 2012 American Society for Histocompatibility and Immunogenetics. Published by Elsevier Inc. All rights reserved.
http://dx.doi.org/10.1016/j.humimm.2012.11.011

with rs10774671 [10] was also associated with the outcome of hepatitis C virus (HCV) infection [15]. However, the allele associated with susceptibility to infection varied among studies, and the production of different *OAS1* isoforms have not yet been fully investigated [16]. Considering that the interactions between virus and host are complex and cell-type-specific, *OAS1* expression patterns should be characterized in a particular cell type infected by a virus of interest. In particular, host genetic factors affecting the airway defense mechanism against emerging respiratory viral infections, such as severe acute respiratory syndrome (SARS) and avian influenza, which pose potential global threats, should be studied intensively in preparation for future outbreaks.

We previously reported association of *OAS1* polymorphisms with susceptibility to infection by the SARS coronavirus in Vietnamese population [17]. In the present study, we investigated the splice site SNP (rs10774671)-dependent expression of transcript variants and production of functional isoforms of *OAS1* in primary cultured human bronchial epithelial (HBE) cells, a site for replication of many respiratory viruses.

2. Materials and methods

2.1. Cell culture

The ethical committee of National Center for Global Health and Medicine (formerly International Medical Center of Japan) approved the study protocol. Primary cultured HBE cells were obtained from the cancer-free bronchi of surgically resected lungs, after obtaining written informed consent from the individuals concerned, all of whom were Japanese.

We isolated and cultured HBE cells from the resected lung tissue as previously described [18], and cells of passages 3–5 were used in this study. Briefly, HBE cells were seeded at a density of 5×10^5/well onto collagen-coated 6-well Transwell plates (Corning, Corning, NY, USA) and cultured in bronchial epithelial growth medium (BEGM; Biowhittaker, Walkersville, MD, USA) for 24 h. Thereafter, cells were stimulated with 1000 IU/ml IFN-β (Biosource International, Camarillo, CA, USA) for 18 h and then harvested.

2.2. DNA isolation and genotyping of the SNP at the splice acceptor site

Genomic DNA was extracted from HBE cells using the QIAamp DNA Mini Kit (QIAGEN, Hamburg, Germany). The SNP rs10774671 was genotyped utilizing PCR and restriction fragment length polymorphism (RFLP) methods. Genomic DNA was amplified using AmpliTaq Gold DNA polymerase (Applied Biosystems, Foster City, CA, USA) with the primers listed in Supplementary Table 1. The cycling conditions involved 45 cycles at 95 °C for 15 s, 55 °C for 15 s, and 72 °C for 30 s. The PCR products (532 bp) were digested with *Alu* I (New England Biolabs, Ipswich, MA, USA) at 37 °C for 2 h, and were then electrophoresed on 3% agarose gels including ethidium bromide. Genotypes were determined by the size of the digested PCR products observed upon visualization of the gels (306, 181, 33, and 12 bp for the G allele and 255, 181, 51, 33, and 12 bp for the A allele).

2.3. Real-time reverse transcription (RT)-PCR

We selected HBE cells with AA ($n = 6$), AG ($n = 3$), and GG ($n = 2$) genotypes of rs10774671; these cells were stimulated with IFN-β. Total RNA was extracted using an RNeasy Mini Kit (QIAGEN). One microgram of the total RNA was subjected to RT with random nonamers using SuperScript III Reverse Transcriptase (Invitrogen, Carlsbad, CA, USA), as recommended by the manufacturer. Expression of *OAS1* mRNA was analyzed by real-time RT-PCR using Power SYBR Green PCR Master Mix (Applied Biosystems) and CFX96 (Bio-Rad, Hercules, CA, USA) according to the manufacturer's instructions.

Previous reports indicated that *OAS1* can give rise to as many as eight alternatively spliced transcripts [16,19,20]. A primer set common to all transcript variants was used to amplify all *OAS1* transcripts, and transcript-specific primer sets were used to amplify each transcript. Primers and annealing/extension temperatures are listed in Table 1. The cycling conditions were as follows: initial activation of the Taq DNA Polymerase for 10 min at 95 °C, followed by 40 cycles of 15 s denaturation at 95 °C, and annealing and extension for 1 min at the appropriate temperature. Specific amplification of the target was confirmed by a single peak in the dissociation curve and by visualization of the expected size of RT-PCR products on an agarose gel.

To compare the mRNA copy numbers among transcript variants, the absolute quantification method was used [21]. Isoform-specific RT-PCR products containing the target sequences, amplified with primers in Supplementary Table 1, were purified using the Wizard PCR Preps DNA Purification System (Promega, Fitchburg, WI, USA). Their copy numbers were calculated from the concentration of DNA determined by measuring absorbance at 260 nm. The standard curve was generated with serial 5-fold dilutions of each of the RT-PCR products. The linear dependence of the threshold cycles was confirmed from the concentration of the templates. We used the β-actin gene (primers in Supplementary Table 1) to normalize

Table 1
OAS1 isoforms and real-time RT-PCR conditions.

Serial number	Isoform	GenBank accession no.	Expected protein sizes (kDa)	Real-time RT-PCR primers	Nucleotide sequences (5′ → 3′)	Annealing and extension temperature (°C)
1	p42	NM_002534.2	41.7	Forward	ACCTGAGAAGGCAGCTCACGAAAC	60
				Reverse	CAGGGAGGAAGCAGGAGGTCTCAC	
2	p46	NM_016816.2	46.0	Forward	ACCTGAGAAGGCAGCTCACGAAAC	68
				Reverse	ATCGTCTGTACTGTTGCTTTCAGCC	
3	p23	AK301498.1	22.8	N/T*		
4	p35	AK300346	35.4	Forward	CTCATCCGCCTAGTCAAGCAC	60
				Reverse	CCAAGGCACTGTACCTGTATCC	
5	p44a	CF272298	44.1	Forward	ACCTGAGAAGGCAGCTCACGAAAC	66
				Reverse	CATTTCCACCACTTGTTAGCTGATGTC	
6	p52	AY730627.1	52.1	Forward	ACCTGAGAAGGCAGCTCACGAAAC	68
				Reverse	ATCGTCTGTACTGTTGCTTTCAGCA	
7	p48	NM_001032409.1	47.4	Forward	ACCTGAGAAGGCAGCTCACGAAAC	68
				Reverse	GCTGCCTGGAGTGTGCTGGGTCAG	
8	p44b	AJ629455.1	43.9	Forward	ACCTGAGAAGGCAGCTCACGAAAC	60
				Reverse	TAGTTCCTTCTGCCAACCAGTGTG	

* Not tested.

OAS1 expression. Fold-changes of total *OAS1* expression with IFN-β and relative mRNA amounts of each transcript with respect to the amount of mRNA for the p42 transcript in AA cells without stimulation of IFN-β were calculated. Data are expressed as the mean ± standard error of the mean (SEM).

2.4. Immunoblot analysis

HBE cells with AA ($n = 8$), AG ($n = 3$), and GG ($n = 2$) genotypes of rs10774671 were stimulated with IFN-β and harvested with lysis buffer Complete Lysis-M, EDTA-free buffer (Roche Applied Science, Penzberg, Germany). The total protein concentration in each sample was measured using the BioRad Protein Assay (BioRad). Equal amounts of total protein from each lysate (20 μg/lane) was resuspended in SDS buffer (125 mM Tris–HCl, pH 6.8, 10% glycerol, 2% SDS, 1.55% dithiothreitol, and 0.1% bromophenol blue), boiled for 5 min, and analyzed on a 10% SDS–PAGE gel (e-PAGEL; ATTO, Tokyo, Japan). Resolved proteins were transferred to a polyvinylidene difluoride membrane (Millipore, Billerica, MA, USA). After blocking the membrane in Tris-buffered saline with 0.1% Tween 20 and 2% blocking reagent at 4 °C overnight, blots were hybridized for 1 h at room temperature with primary antibody against the protein fragment (amino acids 80–221) common to all OAS1 isoforms (Sigma–Aldrich, St. Louis, MO, USA; product number, HPA003657), at a dilution of 1:1000. After hybridization with horseradish peroxidase-conjugated secondary antibody, the immunocomplexes were visualized using an ECL Western blotting detection system (GE Healthcare, Little Chalfont, United Kingdom). The intensity of each band was semi-quantitatively determined using a densitometer with the Quantity One 1-D software (BioRad). The same blot was reprobed with anti-β-tubulin monoclonal antibody (Thermo Fisher Scientific, Waltham, MA, USA) as a loading control.

2.5. Rapid amplification of cDNA ends (5′-RACE and 3′-RACE)

RNA ligase-mediated rapid amplification of cDNA ends (RLM-RACE) was carried out using total RNA from IFN-β-stimulated HBE cells with AA or GG genotypes of rs10774671, using the First-Choice RLM-RACE Kit (Ambion, Austin, TX, USA) according to the manufacturer's instructions. Gene-specific primers are listed in Supplementary Table 1. PCR products were purified and sequenced with the BigDye Terminator v3.1 Cycle Sequencing Kit (Applied Biosystems) using a 3100 Genetic Analyzer (Applied Biosystems). PCR products from 3′-RACE were electrophoresed on 2% agarose gels containing ethidium bromide.

2.6. SNP screening of OAS1 gene

Information about SNP genotypes of *OAS1* in the Japanese population from Tokyo (JPT) was obtained from HapMap data sets [22], and was analyzed using Haploview (v. 4.2) [23]. LD blocks were determined using the confidence interval method [24]. Tag SNPs were selected and genotyped from the DNA of study participants.

In addition, we screened genetic polymorphisms from the promoter region [6] to exon 6 of *OAS1*, using 4 DNA samples with genotypes representing the tag SNP. The entire region was amplified using three overlapping PCR products. Primers are listed in Supplementary Table 1. Amplified products were purified and sequenced using appropriate inner primers as described above.

2.7. DNA fragmentation ELISA

HBE cells with AA ($n = 5$) and GG ($n = 3$) genotypes of rs10774671 were stimulated with or without IFN-β (1000 IU/ml) for 12 h, were further treated with 5×10^{-8} M neutrophil elastase (NE; Elastin Products Company, Owensville, MO, USA) for 6 h. Then, cells were pelleted and lysed, and apoptosis assessed using a cell death detection ELISA system (Cell Death Detection ELISA PLUS; Roche Applied Science). Enrichment for mono- and oligonucleosomes released into the cytoplasmic fractions of cell lysates was detected by biotinylated antihistone- and peroxidase-coupled anti-DNA antibodies. The relative absorbance ratio (absorbance of sample cells/absorbance of control cells) was calculated in triplicate, and used as a parameter of DNA fragmentation.

2.8. Statistical analysis

All data were expressed as mean ± SEM. To assess the effect of the number of A (or G) alleles on expression levels of transcript variants, a linear regression model was applied (JMP, version 9.0.0; SAS Institute Inc., Cary, NC, USA). Relative absorbance ratio from the apoptosis assay was analyzed by the unpaired Student's *t*-test. Differences were considered to be statistically significant when $p < 0.05$.

3. Results

3.1. Difference in OAS1 expression between AA, AG, and GG genotypes

According to previous reports, *OAS1* gives rise to eight alternatively spliced transcripts [16,19,20], and the corresponding gene products with various molecular weights are shown in Fig. 1 and Table 1. Supplementary Fig. 1 shows the results of RT-PCR with primer sets designed to specifically amplify each transcript variant. We did not detect the p23 transcript in HBE cells with any of the three genotypes.

We next analyzed the total and transcript-specific expression of *OAS1* in the presence or absence of IFN-β stimulation by real-time RT-PCR (Fig. 2). When HBE cells were stimulated with IFN-β, total *OAS1* expression was increased up to 20-fold, irrespective of genotype ($p = 0.432$). Of the splicing variants, p42 was the main transcript expressed in HBE cells with the AA genotype, whereas p46 transcripts were predominant in those with the GG genotype. Expression of the p46 transcript was significantly higher in proportion to the number of G alleles carried by HBE cells, under both unstimulated and stimulated conditions ($p < 0.001$, $p < 0.001$). By contrast, expression of the p42, p44a (alternate exon in intron 5), p52, and p48 transcripts was all higher in proportion to the number of A alleles present in the cells, under both unstimulated and stimulated conditions (p42: $p < 0.001$, $p < 0.001$; p44a: $p = 0.014$,

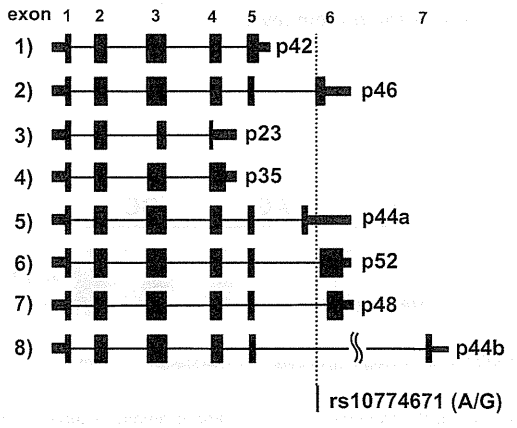

Fig. 1. Schematic representation of *OAS1* transcript variants. Alternatively spliced exons, the predicted protein size, and the position of the SNP at the splice acceptor site (rs10774671) are shown. The number in parenthesis indicates each transcript, corresponding to that in Table 1. Coding regions are indicated by wide rectangles, noncoding regions by narrow rectangles, and introns by lines. We designated the isoform with an alternate exon in intron 5 as p44a, and that with exon7 as p44b.

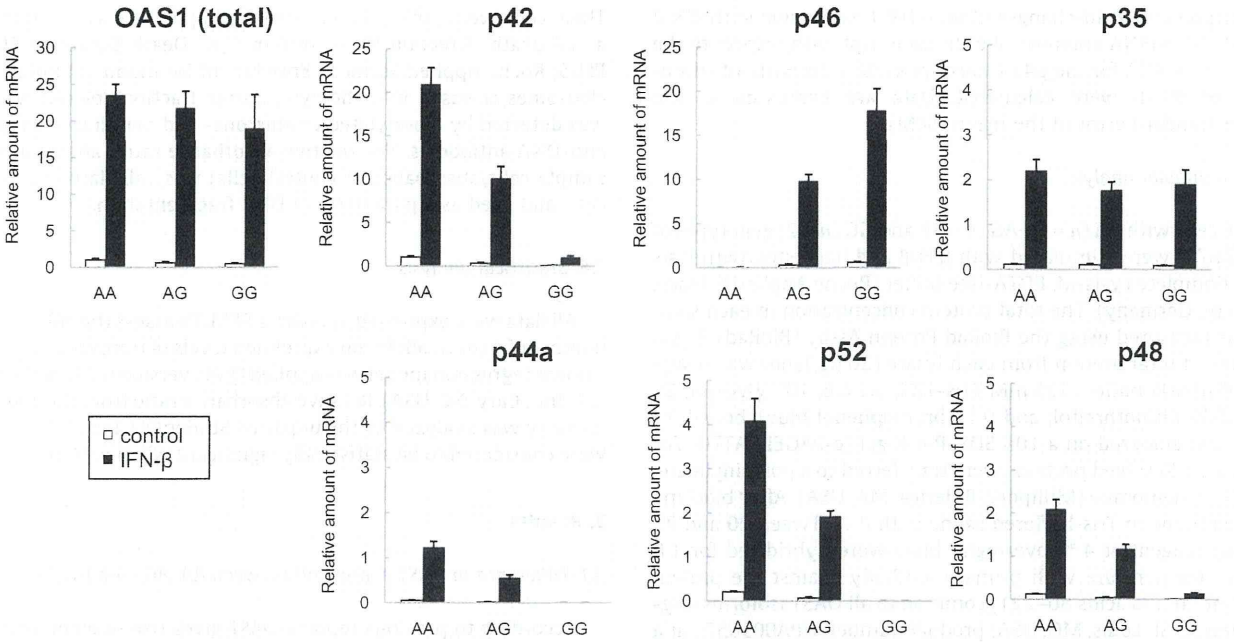

Fig. 2. Difference in the amount of transcript variants among genotypes in HBE cells. The expression of total *OAS1* and that of each individual transcript variant in HBE cells with the AA ($n = 6$), AG ($n = 3$), or GG ($n = 2$) genotypes of rs10774671 was obtained by real-time RT-PCR. Fold-inductions of total *OAS1* expression by IFN-β, and the relative mRNA amounts of each transcript over that of the p42 transcript in AA cells without stimulation of IFN-β are shown as mean ± SEM.

$p < 0.001$; p52: $p < 0.001$, $p = 0.013$; p48: $p < 0.001$, $p = 0.001$). Expression of the p35 transcript was not associated with either allele under both conditions ($p = 0.245$, $p = 0.495$). We did not quantify the p44b transcript containing exon 7 because the threshold cycle number was high and non-specific PCR amplification was observed.

Immunoblot analysis demonstrated expression of the p46 isoform and a low level of p42 in HBE cells with the GG and AG genotypes; another faint band slightly smaller than p46 was also detected. In cells with the AA genotype, only the p42 isoform was distinctly observed (Fig. 3). To compare the protein levels with the corresponding mRNA expression levels, the band intensity corresponding to each protein isoform was semi-quantified. While the p46 transcript was expressed approximately 20-fold more than the p42 transcript at the mRNA level in the GG cells stimulated with IFN-β, the p46 isoform was expressed only 2.2-fold more than the p42 isoform at the protein level.

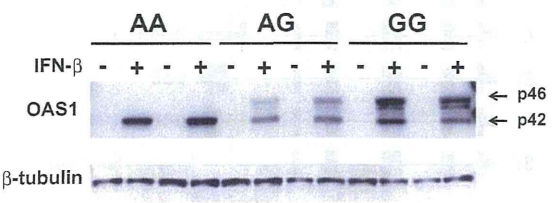

Fig. 3. Difference in the expression of *OAS1* isoforms among genotypes. Western blotting was performed using antibody against the epitope common to all isoforms of OAS1. HBE cells with AA ($n = 8$), AG ($n = 3$), and GG ($n = 2$) genotypes of rs10774671 were analyzed, and the isoform expression pattern was the same in each genotype. Two representative results in each genotype are shown. As a loading control, the same blot was reprobed with anti-β-tubulin monoclonal antibody (bottom part).

3.2. Identification of the transcription start site of OAS1 in cells with the AA and GG genotypes

Using 5′-RACE, we found that the transcription start site of *OAS1* was 81 bp upstream of the translation start site in IFN-β-stimulated HBE cells with the AA and GG genotypes, indicating that the transcription start site did not differ between the genotypes. Using the 3′-RACE method, we showed that the p42, p48, and p52 transcripts were present in HBE cells with the AA genotype, while only the p42 and p46 transcripts were identified in those with the GG genotype (Supplementary Fig. 2). No other novel transcripts were amplified.

3.3. Search for other genetic polymorphisms and LD structures of OAS1

To search for other variants which may influence gene expression, we further analyzed nucleotide sequences throughout the region from the promoter to exon 6 and investigated the LD structure of *OAS1*. We selected rs3741981 (non-synonymous; exon 3), rs4766662 (intron 1), rs2240190 (intron 1), and rs10774671 as tag SNPs for genotyping. The exon 3 SNP was in complete LD with rs10774671 ($D' = 1$, $r^2 = 0.38$). The minor allele frequency of rs4766662 was less than 5%, while rs2240190 was not in LD with rs10774671 ($D' = 0.4$, $r^2 = 0.13$).

The SNP genotypes indicated that only SNPs in the region between intron 3 and exon 6 were in strong LD ($r^2 > 0.8$) with rs10774671. The LD block was bordered by exon 3, and we did not identify any SNP in strong LD with rs10774671 in the region extending from the promoter to intron 2. The LD pattern derived in our study was consistent with that obtained from the HapMap data (Supplementary Fig. 3).

3.4. DNA fragmentation assay

Since a previous report [7] suggested that the p48 isoform potentiates apoptosis through the BH3 domain in its specific C-ter-

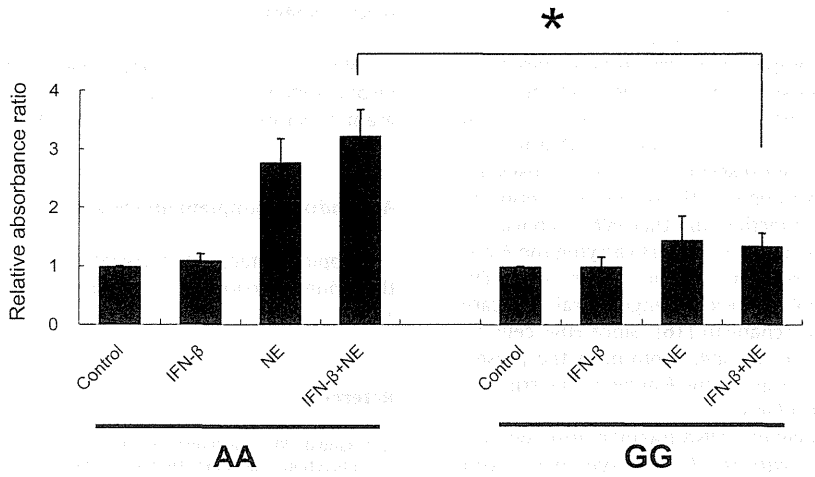

Fig. 4. Difference in DNA fragmentation between AA and GG genotypes. HBE cells with AA ($n = 5$) or GG ($n = 3$) genotypes were stimulated with IFN-β (1000 IU/ml) for 12 h and/or with NE (5×10^{-8} M) for 6 h. With an apoptosis determination kit, relative absorbance ratios (absorbance of sample cells/absorbance of control cells) were obtained and shown as mean ± SEM. Experiments were performed in triplicate. Statistically significant: $^{*}p < 0.05$.

minal, HBE cells were pretreated with IFN-β and further incubated with NE, an apoptosis-inducing agent. Although NE itself did not affect *OAS1* expression, as assessed by immunoblot analysis (data not shown), treatment with NE and IFN-β caused a larger amount of DNA fragmentation in cells with the AA genotype than in those with the GG genotype ($p = 0.021$). The genotype-dependent difference caused by NE in the absence of IFN-β did not reach significant levels ($p = 0.068$, Fig. 4).

4. Discussion

In this study, we investigated the differential effects of a splice site SNP on expression of transcript variants and production of functional isoforms of *OAS1* in primary cultured bronchial epithelial cells isolated from human lung, a major site of replication for respiratory viruses. We clearly demonstrated the G allele-dependent expression of the p46 isoform and the A allele-dependent expression of the p42, p44a, p48, and p52 transcripts. Expression of the p35 transcript did not differ among genotypes.

The G allele-dependent expression of p46 and the A allele-dependent expression of p48 and p52 in HBE cells were consistent with the pioneering report of Bonnevie-Nielsen et al. using human lymphocytes [10]. Prior to their report, such a common splice site SNP had not been identified, and the expression patterns of *OAS1* transcript variants had been assumed to be cell-type specific [25,26].

Furthermore, recent RNA sequencing studies using lymphoblast cell lines revealed that not only p48 and p52 transcripts but also p42 and p44a transcripts are expressed when the A allele is present [19,27]. We confirmed these observations in primary cultured HBE cells. However, the read-through transcript of intron 4 was amplified with the full exon 3 (p35 transcript). The short exon 3 using the alternative splice acceptor site within the exon 3 (p23 transcript) reported in lymphoblast cell lines [19] was not observed in our study.

The total amount of *OAS1* mRNA expression appeared to be slightly lower in proportion to the number of G alleles present, but this tendency was not statistically significant. In a previous study on HIV patients, significantly lower expression of *OAS1* was observed in peripheral blood mononuclear cells carrying the G allele of rs3177979, which is in LD with the G allele of rs10774671 [28]. Conversely, there was a 1.9-fold higher expression in lymphoblastoid cell lines with the GG genotype of rs10774671 than in those with the AG genotype [19]. This discrepancy may have been caused by differences in ethnicity or cell type.

Since the transcription start site was the same for transcripts arising from the A allele and the G allele, and because there was no SNP in the 5′-region of the gene that was in strong LD with rs10774671 according to both our SNP screening and analyses of HapMap data, the transcriptional activity resulting in each transcript variant is presumably similar. Thus, their expression levels would be expected to be determined by the efficiency of splicing and mRNA stability.

Immunoblot analysis revealed that the p46 isoform, and a lower level of p42, were detected in cells with the GG genotype. Interestingly, the amount of p42 isoform was about half that of the p46 isoform in the GG cells at the protein level, although mRNA expression of the p42 transcript was markedly lower than that of the p46 transcript in those cells. Laronde et al. reported that the p42 transcript accounted for 5% of the total *OAS1* transcripts in a lymphoblast cell line with a GG genotype, as determined by RNA sequencing [19]; this was in accord with the results obtained from our absolute quantification method. The translational efficiency may differ between p42 and p46 transcripts because they have distinct 3′-UTR sequences that may differentially bind to RNA-binding proteins [29] or to micro RNAs [30]. In Daudi lymphoid cells with a GG genotype [10], only the p46 isoform was detected [26]. Therefore, expression of the p42 isoform in cells bearing a GG genotype may be specific to the cell type, presumably through tissue-specific regulation of alternative splicing [31].

Another band slightly smaller than p46 was observed in the G allele-carrying cells. A similar band was also visible in Daudi cells with the GG genotype [26]. Thus far, the isoform corresponding to this size has not been identified, and we did not find any novel transcript by 3′-RACE. The band may indicate some degradation of the p46 isoform, although there is no evidence that the C-terminal tail contains a cleavage site.

We predominantly detected the p42 isoform, but not p46 in the cells with the AA genotype, under the same immunoblotting condition. The other isoforms (p35, p44a, p48, and p52), of which the transcripts could be amplified in the AA cells by real-time RT-PCR, were not detected either, possibly because of their low expression levels.

Only a few studies have been conducted on the differences in the function of different isoforms. Bonnevie-Nielsen et al. reported

that the total enzyme activity of *OAS1* in unstimulated lymphocytes was highest in individuals with the GG genotype, intermediate in those with the AG genotype, and lowest in those with the AA genotype. They raised the possibility that the p46 isoform, arising from the G allele, has higher enzymatic activity than the p48 and p52 isoforms arising from the A allele. This suggests that individuals carrying the A allele are more susceptible to some viruses; consequently, Lim et al. demonstrated that the A allele was associated with susceptibility to WNV infection and that WNV replicated to higher levels in lymphoid tissues from donors carrying the A allele [14]. Lin et al. reported that p42 and p46, but not the other *OAS1* isoforms (p44b, p48, and p52), blocked dengue viral replication via an RNase L-dependent mechanism [16]. Since HBE cells produce a considerable amount of the p42 isoform in the presence of the AA genotype, functional roles of the A allele are worth reconsidering in respiratory virus infection.

In our study, NE-induced cellular DNA fragmentation was preferentially found in HBE cells with the AA genotype when stimulated with IFN-β. NE is a major apoptotic inducer in inflamed airway epithelium, and Suzuki et al. showed molecular mechanisms of leukocyte elastase-induced apoptosis in HBE cells [32]. We also found that NE increased the level of annexin-V staining in an immortalized HBE cell line, BEAS-2B (unpublished observation). However, we could not further investigate other key features of apoptosis than DNA fragmentation in the present study, because the number of experiments using primary cultured cells had limitations. Since the p48 isoform arising from the A allele was previously shown to have proapoptotic activity independent of RNase L activation [7], it is conceivable that the increased DNA fragmentation in HBE cells with the AA genotype is attributed to this unique activity of the p48 isoform that is presumably absent in the cells with the GG genotype. RNase L activation may not be involved in the difference observed in the present study because OAS enzymatic activity is detectable in the presence of exogenous dsRNA [4]. However, it remains elusive whether genotypic differences in DNA fragmentation was derived from the p48 isoform, because its protein expression was not detected by the sensitivity of Western blotting. Alternatively, the predominant p42 isoform in cells bearing the AA genotype may be related to DNA fragmentation through an unknown mechanism. It is generally known that apoptosis can contribute to protection against viral infection by killing virus-infected cells, but it may also serve as a mechanism for virus-induced tissue injury and progression of disease [33]. We have postulated that HBE cells carrying the A allele are more likely to inhibit spreading of the virus infection through promotion of apoptosis of virus-infected cells; thus, the A allele is associated with resistance to SARS infection [17]. Our findings indicate a requirement for further understanding of allele-specific functions other than classical enzymatic activity of OAS isoforms.

The G allele of rs10774671 is possibly an ancestral type because it had been identified in hominoid primates (*Pan troglodytes*), Old World monkeys (*Macaca mulatta*), and New World monkeys (*Callithrix jacchus*), according to the sequence data from public databases. Additionally, a recent study reported that the region carrying the splice site variant was neutrally evolving [20]. It is intriguing to speculate that the G to A substitution of rs10774671 generated isoforms with low enzymatic activity and high apoptosis-inducing activity, resulting in maintaining the balance between resistance and susceptibility to viral infection.

In conclusion, we have characterized the rs10774671 SNP-dependent expression profile of *OAS1* transcript variants and isoforms with possibly different functions in primary cultured HBE cells. Our findings may lead to an improved understanding of the association of *OAS1* gene with susceptibility to infection with respiratory viruses.

Acknowledgments

We thank Keiko Wakabayashi and Fumi Toshioka for their technical assistance in the study. This work was partly supported by a grant of National Center for Global Health and Medicine.

Appendix A. Supplementary data

Supplementary data associated with this article can be found, in the online version, at http://dx.doi.org/10.1016/j.humimm.2012.11.011.

References

[1] Randall RE, Goodbourn S. Interferons and viruses: an interplay between induction, signalling, antiviral responses and virus countermeasures. J Gen Virol 2008;89:1–47.
[2] Sadler AJ, Williams BR. Interferon-inducible antiviral effectors. Nat Rev Immunol 2008;8:559–68.
[3] Hovanessian AG, Justesen J. The human 2'-5'oligoadenylate synthetase family: unique interferon-inducible enzymes catalyzing 2'-5' instead of 3'-5' phosphodiester bond formation. Biochimie 2007;89:779–88.
[4] Kristiansen H, Gad HH, Eskildsen-Larsen S, Despres P, Hartmann R. The oligoadenylate synthetase family: an ancient protein family with multiple antiviral activities. J Interferon Cytokine Res 2011;31:41–7.
[5] Chakrabarti A, Jha BK, Silverman RH. New insights into the role of RNase L in innate immunity. J Interferon Cytokine Res 2011;31:49–57.
[6] Justesen J, Hartmann R, Kjeldgaard NO. Gene structure and function of the 2'-5'-oligoadenylate synthetase family. Cell Mol Life Sci 2000;57:1593–612.
[7] Ghosh A, Sarkar SN, Rowe TM, Sen GC. A specific isozyme of 2'-5' oligoadenylate synthetase is a dual function proapoptotic protein of the Bcl-2 family. J Biol Chem 2001;276:25447–55.
[8] Domingo-Gil E, Esteban M. Role of mitochondria in apoptosis induced by the 2–5A system and mechanisms involved. Apoptosis 2006;11:725–38.
[9] Castelli JC, Hassel BA, Maran A, Paranjape J, Hewitt JA, Li XL, et al. The role of 2'-5' oligoadenylate-activated ribonuclease L in apoptosis. Cell Death Differ 1998;5:313–20.
[10] Bonnevie-Nielsen V, Field LL, Lu S, Zheng DJ, Li M, Martensen PM, et al. Variation in antiviral 2',5'-oligoadenylate synthetase (2'5'AS) enzyme activity is controlled by a single-nucleotide polymorphism at a splice-acceptor site in the OAS1 gene. Am J Hum Genet 2005;76:623–33.
[11] Burgner D, Jamieson SE, Blackwell JM. Genetic susceptibility to infectious diseases: big is beautiful, but will bigger be even better? Lancet Infect Dis 2006;6:653–63.
[12] Mashimo T. A nonsense mutation in the gene encoding 2'-5'-oligoadenylate synthetase/L1 isoform is associated with West Nile virus susceptibility in laboratory mice. Proc Natl Acad Sci USA 2002;99:11311–6.
[13] Perelygin AA. Positional cloning of the murine flavivirus resistance gene. Proc Natl Acad Sci USA 2002;99:9322–7.
[14] Lim JK, Lisco A, McDermott DH, Huynh L, Ward JM, Johnson B, et al. Genetic variation in OAS1 is a risk factor for initial infection with West Nile virus in man. PLoS Pathog 2009;5:e1000321.
[15] Knapp S, Yee LJ, Frodsham AJ, Hennig BJ, Hellier S, Zhang L, et al. Polymorphisms in interferon-induced genes and the outcome of hepatitis C virus infection: roles of MxA, OAS-1 and PKR. Genes Immun 2003;4:411–9.
[16] Lin RJ, Yu HP, Chang BL, Tang WC, Liao CL, Lin YL. Distinct antiviral roles for human 2',5'-oligoadenylate synthetase family members against dengue virus infection. J Immunol 2009;183:8035–43.
[17] Hamano E, Hijikata M, Itoyama S, Quy T, Phi NC, Long HT, et al. Polymorphisms of interferon-inducible genes OAS-1 and MxA associated with SARS in the Vietnamese population. Biochem Biophys Res Commun 2005;329:1234–9.
[18] Gray TE, Guzman K, Davis CW, Abdullah LH, Nettesheim P. Mucociliary differentiation of serially passaged normal human tracheobronchial epithelial cells. Am J Respir Cell Mol Biol 1996;14:104–12.
[19] Lalonde E, Ha KC, Wang Z, Bemmo A, Kleinman CL, Kwan T, et al. RNA sequencing reveals the role of splicing polymorphisms in regulating human gene expression. Genome Res 2011;21:545–54.
[20] Cagliani R, Fumagalli M, Guerini FR, Riva S, Galimberti D, Comi GP, et al. Identification of a new susceptibility variant for multiple sclerosis in OAS1 by population genetics analysis. Hum Genet 2012;131:87–97.
[21] Leong DT, Gupta A, Bai HF, Wan G, Yoong LF, Too HP, et al. Absolute quantification of gene expression in biomaterials research using real-time PCR. Biomaterials 2007;28:203–10.
[22] A haplotype map of the human genome. Nature 2005;437:1299–320.
[23] Barrett JC, Fry B, Maller J, Daly MJ. Haploview: analysis and visualization of LD and haplotype maps. Bioinformatics 2005;21:263–5.
[24] Gabriel SB, Schaffner SF, Nguyen H, Moore JM, Roy J, Blumenstiel B, et al. The structure of haplotype blocks in the human genome. Science 2002;296:2225–9.

[25] Benech P, Merlin G, Revel M, Chebath J. 3' end structure of the human (2′-5′) oligo A synthetase gene: prediction of two distinct proteins with cell type-specific expression. Nucleic Acids Res 1985;13:1267–81.
[26] Chebath J, Benech P, Hovanessian A, Galabru J, Revel M. Four different forms of interferon-induced 2′,5′-oligo(A) synthetase identified by immunoblotting in human cells. J Biol Chem 1987;262:3852–7.
[27] Pickrell JK, Marioni JC, Pai AA, Degner JF, Engelhardt BE, Nkadori E, et al. Understanding mechanisms underlying human gene expression variation with RNA sequencing. Nature 2010;464:768–72.
[28] Rotger M, Dang KK, Fellay J, Heinzen EL, Feng S, Descombes P, et al. Genome-wide mRNA expression correlates of viral control in CD4+ T-cells from HIV-1-infected individuals. PLoS Pathog 2010;6:e1000781.
[29] Glisovic T, Bachorik JL, Yong J, Dreyfuss G. RNA-binding proteins and post-transcriptional gene regulation. FEBS Lett 2008;582:1977–86.
[30] Fabian MR, Sonenberg N, Filipowicz W. Regulation of mRNA translation and stability by microRNAs. Annu Rev Biochem 2010;79:351–79.
[31] Heinzen EL, Ge D, Cronin KD, Maia JM, Shianna KV, Gabriel WN, et al. Tissue-specific genetic control of splicing: implications for the study of complex traits. PLoS Biol 2008;6:e1.
[32] Suzuki T, Yamashita C, Zemans RL, Briones N, Van Linden A, Downey GP. Leukocyte elastase induces lung epithelial apoptosis via a PAR-1-, NF-kappaB-, and p53-dependent pathway. Am J Respir Cell Mol Biol 2009;41:742–55.
[33] Kaminskyy V, Zhivotovsky B. To kill or be killed: how viruses interact with the cell death machinery. J Intern Med 2010;267:473–82.